Journal of Energy Storage 51 (2022) 104444

Contents lists available at ScienceDirect

Journal of Energy Storage

journal homepage: www.elsevier.com/locate/est

Research papers

Operational benefit of transforming cascade hydropower stations into pumped hydro energy storage systems

Parinaz Toufani, Emre Nadar, Ayse Selin Kocaman *

Department of Industrial Engineering, Bilkent University, 06800 Ankara, Turkey

ARTICLE INFO

Keywords:
Cascade hydropower stations
Pumped hydro energy storage
Streamflow rate
Negative electricity prices
Stochastic dynamic program

ABSTRACT

This study evaluates the potential benefit of retrofitting existing conventional cascade hydropower stations (CCHSs) with reversible turbines so as to operate them as pumped hydro energy storage (PHES) systems. We examine the energy generation and storage problem for a CCHS with two connected reservoirs that can be transformed into a PHES system in a market setting where the electricity price can be negative. We formulate this problem as a stochastic dynamic program (SDP) under uncertainty in the streamflow rate and electricity price. We analytically derive an upper bound on the profit improvement that can be obtained from the PHES transformation. We conduct numerical experiments with data-calibrated time series models and observe that the PHES system provides a greater benefit under more limited streamflow conditions or more frequently observed negative prices.

1. Introduction

A typical PHES system stores and generates electricity by exchanging water flow between two reservoirs located at different altitudes. When the electricity price is low due to an excess energy supply, energy can be stored in the form of hydraulic potential energy by pumping water from the lower reservoir to the upper reservoir. When the electricity price is high due to a surge in energy demand, energy can be generated by releasing the water stored in the upper reservoir to the lower reservoir. PHES is an attractive storage option with promising round-trip efficiencies (70% to 80%), short response times (minutes to seconds), and long useful lifetimes (50 to 100 years) [1–3].

As part of the International Renewable Energy Agency's global roadmap, the currently installed capacity of PHES needs to be doubled, reaching 325 GW by 2050 [4]. A major challenge in new PHES installations, however, is the need for quite specific site conditions such as water access and favorable topography [5]. This challenge draws the attention of the PHES investors to the existing CCHSs in which these conditions are already satisfied. Current trends show that it is often possible to retrofit the CCHSs with reversible turbines to endow them with pumping capability [6]. In this paper, we evaluate the potential benefit of rehabilitating an existing CCHS to operate it as a PHES system in a market setting where the electricity price can be negative. We formulate the real-time decision making process of the PHES system as an SDP, by taking into account uncertainties in the streamflow incoming to the hydropower system as well as in the electricity price and by constructing data-calibrated time series models to include these uncertainties.

Previous research dealing with the optimization of PHES systems focus on finding the optimal size and configurations of the new systems [7–12] and the optimal operating rules of the existing systems [2,13–23]. Most of these studies develop deterministic optimization models or scenario-based stochastic programming approaches. However, deterministic models do not take uncertainty into account. Stochastic programming approaches, on the other hand, require scenario generation in advance, which may fail to adequately capture the impact of exogenous events on sequential decision-making. Such approaches, for a particular scenario, violate the nonanticipativity condition by allowing the controller to see the future outcomes [24]. Alternatively, SDPs allow uncertainties to be resolved only when the controller progresses in time, while enabling adaptive decisions based on the real-time realizations of uncertainties. SDPs also offer a precise mathematical framework to analytically derive structural results by capturing multidimensional dynamics and uncertainty inherent in the problem [25].

To our knowledge, however, only a few studies have developed SDPs in the PHES literature. Löhndorf et al. [17] study the energy commitment and storage problem for a PHES system by formulating a multi-stage stochastic program for intraday decisions and an SDP for interday decisions. Avci et al. [23] examine the integrated operations of a hybrid energy system that includes a wind farm and a PHES facility (simpler than our PHES configuration in this paper). They

* Corresponding author.
E-mail addresses: parinaz.toufani@bilkent.edu.tr (P. Toufani), emre.nadar@bilkent.edu.tr (E. Nadar), selin.kocaman@bilkent.edu.tr (A.S. Kocaman).

https://doi.org/10.1016/j.est.2022.104444
Received 19 October 2021; Received in revised form 10 February 2022; Accepted 14 March 2022
Available online 4 April 2022

model the problem as an SDP and characterize the optimal policy structure. However, these papers present no result for the potential value of operating a CCHS as a PHES system.

Despite the widespread practice of rehabilitating CCHSs as PHES systems [26,27], as far as we are aware, only a few studies quantify the value of such rehabilitation. Bozorg Haddad et al. [18] formulate nonlinear programs to examine the advantages of converting CCHSs to PHES systems by ignoring uncertainties in the electricity price and streamflow rate. Ak et al. [20] study the same problem by developing a nonlinear program and solving it as many times as the number of scenarios generated to take the price uncertainty into account and by ignoring the streamflow uncertainty. Finally, Ribeiro et al. [28] study a similar problem by formulating a deterministic dynamic program.

The main contributions of this paper are as follows:

- Our study is the first to assess the potential benefit of transforming an existing CCHS into a PHES system via an SDP framework that captures the price and streamflow uncertainties as well as the nonlinear dynamics of the problem. With our SDP framework, we are the first to offer a theoretical upper bound on the profit improvement that can be achieved with the pumping capability in the CCHS.
- We conduct numerical experiments with data-calibrated time series models to provide insights into the optimal operations and profits of the CCHS as well as the PHES system in different environments.
- We show the benefit of taking into account the price and streamflow uncertainties by comparing the results of our stochastic solution approach with a deterministic one.

This paper is organized as follows: Section 2 formulates the energy generation and storage problem for a PHES system. Section 3 presents our theoretical upper bound and numerical results for the benefit of pumping capability. Section 4 measures the value of including randomness in our formulation. Section 5 offers a summary and the conclusions.

2. Problem formulation

We consider a CCHS with two reservoirs at different altitudes where energy can be generated by releasing water from the upper reservoir to the lower reservoir or from the lower reservoir to the stream bed. There is a natural streamflow incoming to the upper reservoir. Any excess amount of the streamflow (and any excess amount of the water pumped in the PHES system) spills from the upper reservoir and feeds the lower reservoir. Utilizing a reversible turbine between the cascading reservoirs, one can transform this CCHS into a PHES system in which energy can be stored by pumping water from the lower reservoir to the upper reservoir. Fig. 1 illustrates one such PHES system. Since the PHES system includes the CCHS as a special case when the pumping capability is disabled, we present below the SDP formulation of the PHES system. In order to quantify the value of transforming the CCHS into a PHES system, we compare the expected total cash flows that result from the transactions of these systems with an electricity market. We presume that the system operations are unable to influence the market price, that is, the operator is a price-taker. Such market settings appear in many related papers; see, for example, [18–20,25,29], and [30].

The amount of energy that can be generated by releasing a unit volume of water from any reservoir equals the multiplication of the water density (ρ), the gravitational constant (g), the potential head of the hydropower station, and the electricity conversion efficiency of the turbine. The efficiency depends on the water flow rate and the potential head available. The potential head is usually determined based on the constructed wall of the dam and the topography of the site. We assume that the vertical height of a waterfall is measured from the intake to the turbine, leading to constant heads for the upper and lower hydropower stations (h_1 and h_2). This assumption appears in many PHES papers; see, for example, [9,31], and [32]. Nevertheless, our SDP formulation can be easily modified to incorporate a variable head as the water is drawn from the reservoir. Our efficiency calculations are based on an efficiency curve that is a function of the ratio of the water flow rate to the design charge or discharge amount of the pump or turbine. We denote the design discharge amounts of the upper and lower turbines by Q_{RU} and Q_{RL}, respectively, and the design charge amount of the pump by Q_P. We also denote the efficiency functions of the upper and lower turbines in the discharging mode by $\Phi_{RU}(\cdot)$ and $\Phi_{RL}(\cdot)$, respectively, and the efficiency function of the pump in the charging mode by $\Phi_P(\cdot)$. The energy generated by releasing a unit volume of water from the upper reservoir is $\rho g h_1 \Phi_{RU}$, the energy generated by releasing a unit volume of water from the lower reservoir is $\rho g h_2 \Phi_{RL}$, and the energy required to pump a unit volume of water from the lower reservoir is $\rho g h_1 / \Phi_P$. We define C_U and C_L as the maximum amounts of water that can be stored in the upper and lower reservoirs, respectively. We assume no loss of water due to evaporation and no delay or efficiency loss due to vertical or horizontal distances between the reservoirs.

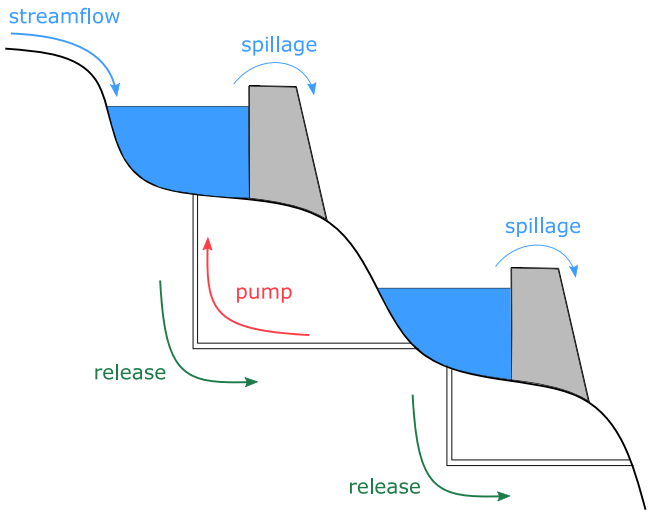

Fig. 1. Illustration of the PHES system.

For the PHES system, we study the energy generation and storage problem via a dynamic model over a finite planning horizon of $\mathcal{T}$ periods. Let $\mathcal{T} := \{1, 2, \ldots, T\}$ denote the set of periods. We denote the accumulated amounts of water in the upper and lower reservoirs at the beginning of period t by x_{ut} and x_{lt}, respectively. Note that $x_{ut} \in [0, C_U]$ and $x_{lt} \in [0, C_L]$. We define r_t as the amount of streamflow incoming to the upper reservoir at the beginning of period t and p_t as the electricity price in period t. We also define $y_t := (r_\kappa, p_\kappa)_{\kappa \le t}$ as the history of the streamflow rate and electricity price, which evolves over time according to an exogenous stochastic process. We include x_{ut}, x_{lt}, and y_t in our state description. In each period t, after observing y_t as well as x_{ut} and x_{lt}, the operator determines the amount of water that will be released from or pumped to the upper reservoir $a_t \in \mathbb{R}$ and the amount of water that will be released from the lower reservoir $b_t \in \mathbb{R}_+$. If $a_t \ge 0$, the water is released from the upper reservoir to the lower reservoir. If $a_t < 0$ (in the PHES system only), the water is pumped from the lower reservoir to the upper reservoir. We thus assume that the reversible turbine can operate in only one mode (either pumping or releasing) within a time period, as widely recognized in the PHES literature dealing with short-term planning problems with hourly periods [15,33,34]. We also assume that if $a_t > 0$ and $b_t > 0$, the water in the lower reservoir is released after the water in the upper reservoir is released. Finally, we assume that $b_t = 0$ if $a_t < 0$. Fig. 2 illustrates the sequence of events in each period.

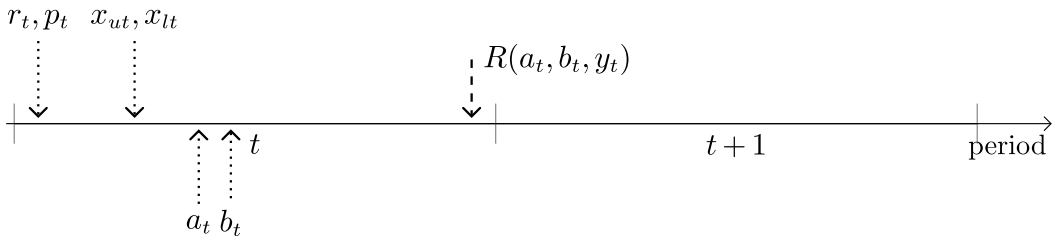

Fig. 2. Sequence of events in each period.

Let $\mathbb{U}(x_{ut}, x_{lt}, y_t)$ denote the set of action pairs (a_t, b_t) that are admissible in state (x_{ut}, x_{lt}, y_t). For any action pair $(a_t, b_t) \in \mathbb{U}(x_{ut}, x_{lt}, y_t)$, the following conditions must hold:

$$-\min\{x_{lt}, Q_P\} \le a_t \le \min\{x_{ut}, Q_{RU}\}$$

and

$$0 \le b_t \le \begin{cases} \min\{x_{lt} + a_t, C_L, Q_{RL}\} & \text{if } a_t \ge 0, \\ 0 & \text{if } a_t < 0. \end{cases}$$

The state variables x_{ut} and x_{lt} evolve over time as in (1), (2a), and (2b).

$$x_{u(t+1)} = \min\{\min\{x_{ut} - a_t, C_U\} + r_{t+1}, C_U\} = \min\{x_{ut} - a_t + r_{t+1}, C_U\}. \tag{1}$$

Let $(x)^+ := \max\{x, 0\}$. If $a_t \ge 0$,

$$x_{l(t+1)} = \min\Big\{\min\{x_{lt} + a_t, C_L\} - b_t + \left(x_{ut} - a_t + r_{t+1} - C_U\right)^+, C_L\Big\}. \tag{2a}$$

If $a_t < 0$,

$$x_{l(t+1)} = \min\Big\{x_{lt} + a_t + \left(x_{ut} - a_t - C_U\right)^+ + \left(\min\{x_{ut} - a_t, C_U\} + r_{t+1} - C_U\right)^+, C_L\Big\}. \tag{2b}$$

In the above formulation, $\left(x_{ut} - a_t - C_U\right)^+$ is the amount of water spilling from the upper reservoir due to the water pumped, and $\left(x_{ut} - a_t + r_{t+1} - C_U\right)^+$ and $\left(\min\{x_{ut} - a_t, C_U\} + r_{t+1} - C_U\right)^+$ are the amounts of water spilling from the upper reservoir due to the water runoff.

The objective is to maximize the expected total cash flow from sales and purchases of energy over the finite horizon. In any period t, if some water is released from the upper or lower reservoir ($a_t \ge 0$ and $b_t \ge 0$), the energy generated is sold to the market. If some water is pumped to the upper reservoir to store energy ($a_t < 0$ and $b_t = 0$), the energy required is purchased from the market. Hence, given the action pair (a_t, b_t) and exogenous state pair y_t, the payoff in period t is formulated in (3).

$$R(a_t, b_t, y_t) = \begin{cases} p_t \rho g \left(a_t \Phi_{RU}\left(a_t/Q_{RU}\right) h_1 + b_t \Phi_{RL}\left(b_t/Q_{RL}\right) h_2\right) & \text{if } a_t \ge 0, \\ p_t \rho g h_1 \left(a_t/\Phi_P\left(a_t/Q_P\right)\right) & \text{if } a_t < 0. \end{cases} \tag{3}$$

A control policy π is the sequence of decision rules $(a_t^\pi(x_{ut}^\pi, x_{lt}^\pi, y_t), b_t^\pi(x_{ut}^\pi, x_{lt}^\pi, y_t))_{t\in\mathcal{T}}$, where x_{ut}^π and x_{lt}^π are the random state variables under policy π, $\forall t \in \mathcal{T}\backslash\{1\}$. We denote the set of all admissible control policies by Π. For any initial state (x_{u1}, x_{l1}, y_1), the optimal expected total cash flow over the finite horizon is given in (4).

$$\max_{\pi\in\Pi} \mathbb{E}\left[\sum_{t\in\mathcal{T}} R\left(a_t^\pi\left(x_{ut}^\pi, x_{lt}^\pi, y_t\right), b_t^\pi\left(x_{ut}^\pi, x_{lt}^\pi, y_t\right)\right) \Big| x_{u1}, x_{l1}, y_1\right]. \tag{4}$$

For each state (x_{ut}, x_{lt}, y_t) in each period $t \in \mathcal{T}$, the optimal profit function $v_t^*(x_{ut}, x_{lt}, y_t)$ can be calculated with the following dynamic programming recursion:

$$v_t^*(x_{ut}, x_{lt}, y_t) = \max_{(a_t,b_t)\in\mathbb{U}(x_{ut},x_{lt},y_t)} \Big\{ R(a_t, b_t, y_t) + \mathbb{E}_{y_{t+1}|y_t}\left[v_{t+1}^*\left(x_{u(t+1)}, x_{l(t+1)}, y_{t+1}\right)\right] \Big\} \tag{5}$$

where $v_T^*(x_{uT}, x_{lT}, y_T) = 0$. This recursion proceeds backward from period T by calculating the optimal actions and profit for each state in each period via a complete enumeration method. For the initial state (x_{u1}, x_{l1}, y_1), $v_1^*(x_{u1}, x_{l1}, y_1)$ is the optimal expected total cash flow over the finite horizon.

3. Results and discussion

3.1. Theoretical bound on the value of PHES

In this section, we establish a theoretical upper bound on the profit improvement that can be achieved with the PHES transformation. Let $\tilde{v}_t^*$ denote the optimal profit function in period t for the CCHS; this can be calculated via the recursion in (5) by restricting the action a_t to be nonnegative for all t. For our upper bound, we assume that the system efficiencies are constants in both charging and discharging modes, and are independent of the amount of water pumped or released throughout the entire planning horizon.

Assumption 1. $\Phi_{RU}\left(a_t/Q_{RU}\right) = \phi_{RU} \in (0, 1]$, $\Phi_P\left(a_t/Q_P\right) = \phi_P \in (0, 1]$, and $\Phi_{RL}\left(b_t/Q_{RL}\right) = \phi_{RL} \in (0, 1]$, $\forall a_t, b_t$.

Theorem 1. *Suppose that Assumption 1 holds. Then,* $\tilde{v}_t^*(x_{ut}, x_{lt}, y_t) \le v_t^*(x_{ut}, x_{lt}, y_t) \le \tilde{v}_t^*(x_{ut}, x_{lt}, y_t) + Q_P \rho g h_1 (T - t)\left(\phi_{RU} \max_{t\le\tau\le T} \overline{p}_\tau - \min_{t\le\tau\le T} \underline{p}_\tau/\phi_P\right)^+$, *where* $p_t \in [\underline{p}_t, \overline{p}_t]$ *and* $\overline{p}_t \ge 0$, *for all* $t \in \mathcal{T}$.

Since the PHES system includes the CCHS as the special case when $a_t \ge 0$, $\forall t$, the optimal profit function of the PHES system is bounded below by that of the CCHS. The upper bound for the optimal profit difference between the PHES system and the CCHS can be viewed as the gap between the revenue obtained by generating and selling energy at full capacity at the maximum possible electricity price and the cost incurred by purchasing and storing energy at full capacity at the minimum possible electricity price, summed over all future periods except the last period (recall that the optimal profit function in period T is zero for both settings). This upper bound is affected by the electricity price and the physical features of the PHES system. A tight upper bound can be obtained in the markets with low volatility in the electricity price and in the systems with low efficiency in the installed turbine/pump. An important implication of this upper bound is that the PHES transformation brings no additional profit if $\min_{1\le\tau\le T} \underline{p}_\tau \ge \phi_{RU}\phi_P \max_{1\le\tau\le T} \overline{p}_\tau$. However, this condition never holds if the electricity price can be negative in some periods.

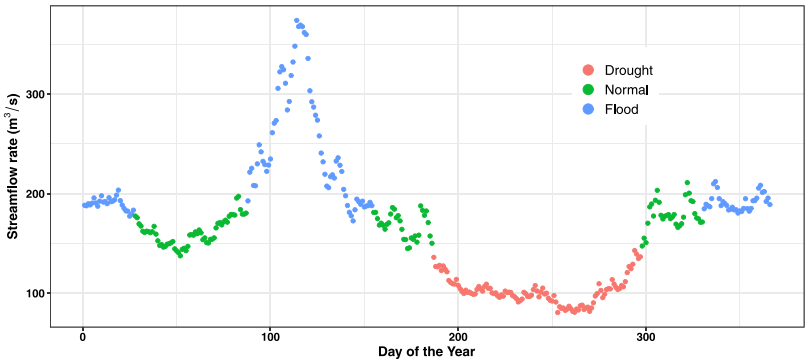

(a) Fort Edward

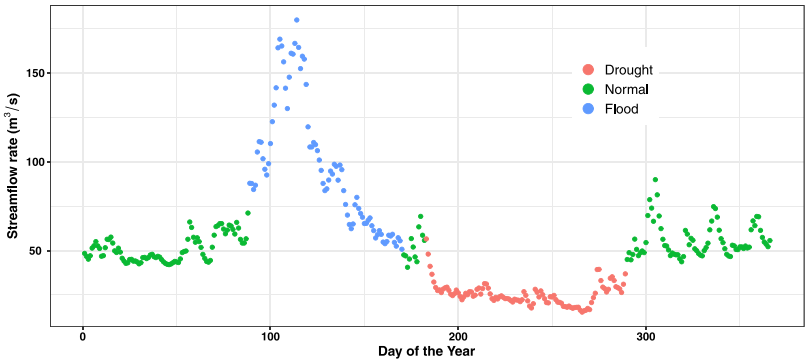

(b) North Creek

Fig. 3. Three clusters for 365 days of the year and the daily average streamflow rates over the years 2000–2019.

3.2. Experimental setup for the numerical study

In our experiments we set the period length to be one hour, as in [9,35], and [36]. For the streamflow rate, we consider two distinct data sets with substantially different rates in the State of New York, the Hudson River at Fort Edward and at North Creek, between the years 2000 and 2019 [37]. We restrict the intraday hourly streamflow rates to stay constant because the data sets display no substantial fluctuation within each day. However, a frequency spectrum analysis of the streamflow rates indicates the significance of daily frequency. Hence, we model the interday streamflow rates by fitting a periodic autoregressive (PAR) model to daily average streamflow rates. Specifically, we partition the 365 days of the year into disjoint clusters of 'normal,' 'drought,' and 'flood' with the fuzzy c-means clustering approach in [38]. Fig. 3 shows these three clusters at Fort Edward and North Creek.

Following Wang et al. [39], we characterize the streamflow rate in each cluster i as following a different autoregressive of order one, AR(1), process: $r_t = \delta_i + \phi_i r_{t-1} + \sigma_i \epsilon_t$, $\forall t \in \mathcal{T}_i$, where $\{\epsilon_t\}_{t\in\mathcal{T}_i}$ are independent standard normal error terms, δ_i is a constant, ϕ_i is the autoregressive coefficient, σ_i is the volatility of white noise, and $\mathcal{T}_i$ is the set of daily periods that belong to cluster i. Table 1 exhibits the parameter estimates of the PAR models at Fort Edward and North Creek.

To incorporate this parametric model into our SDP, we discretize the continuous space of the AR(1) processes: For Fort Edward and North Creek, we restrict the streamflow rate to take values from the sets $\mathcal{R}_F^n := \{75, 100, \ldots, 250\}$ and $\mathcal{R}_N^n := \{20, 45, 70, 95\}$ in the normal flow cluster, the sets $\mathcal{R}_F^d := \{50, 75, \ldots, 200\}$ and $\mathcal{R}_N^d := \{5, 30, 55\}$ in the drought flow cluster, and the sets $\mathcal{R}_F^f := \{100, 125, \ldots, 350\}$ and $\mathcal{R}_N^f := \{25, 50, \ldots, 200\}$ in the flood flow cluster, respectively. We then formulate the AR(1) process of the streamflow rate in each cluster as a different finite-state Markov chain for which we calculate the transition probabilities with the procedure in [40]. For Fort Edward, the transition matrix of the Markov chain in the normal flow cluster is

Table 1
Parameter estimates of the PAR model.

	Fort Edward			North Creek		
Parameters	Normal	Drought	Flood	Normal	Drought	Flood
$\hat{\phi}_i$	0.904	0.939	0.942	0.837	0.839	0.907
$\hat{\sigma}_i$	34.42	19.23	41.96	21.84	13.69	33.69
$\hat{\delta}_i$	168.17	102.68	223.10	52.05	25.87	91.48

$$P_F^n = \begin{array}{c} \\ 75 \\ 100 \\ 125 \\ 150 \\ 175 \\ 200 \\ 225 \\ 250 \end{array} \begin{array}{c} \begin{array}{cccccccc} 75 & 100 & 125 & 150 & 175 & 200 & 225 & 250 \end{array} \\ \begin{bmatrix} .716 & .187 & .076 & .018 & .003 & .000 & .000 & .000 \\ .466 & .273 & .175 & .067 & .016 & .002 & .000 & .000 \\ .229 & .265 & .267 & .163 & .060 & .013 & .002 & .000 \\ .081 & .170 & .271 & .261 & .151 & .053 & .011 & .002 \\ .020 & .072 & .182 & .276 & .253 & .140 & .047 & .011 \\ .003 & .020 & .081 & .193 & .280 & .244 & .129 & .050 \\ .000 & .004 & .024 & .090 & .205 & .282 & .235 & .161 \\ .000 & .000 & .005 & .027 & .099 & .216 & .283 & .369 \end{bmatrix} \end{array},$$

the transition matrix in the drought flow cluster is

$$P_F^d = \begin{array}{c} \\ 50 \\ 75 \\ 100 \\ 125 \\ 150 \\ 175 \\ 200 \end{array} \begin{array}{c} \begin{array}{ccccccc} 50 & 75 & 100 & 125 & 150 & 175 & 200 \end{array} \\ \begin{bmatrix} .791 & .192 & .017 & .000 & .000 & .000 & .000 \\ .340 & .473 & .173 & .014 & .000 & .000 & .000 \\ .051 & .318 & .464 & .155 & .012 & .000 & .000 \\ .002 & .058 & .340 & .452 & .138 & .009 & .000 \\ .000 & .003 & .067 & .361 & .439 & .122 & .008 \\ .000 & .000 & .003 & .078 & .381 & .424 & .114 \\ .000 & .000 & .000 & .004 & .090 & .400 & .506 \end{bmatrix} \end{array},$$

and the transition matrix in the flood flow cluster is

$$P_F^f = \begin{array}{c} \\ 100 \\ 125 \\ 150 \\ 175 \\ 200 \\ 225 \\ 250 \\ 275 \\ 300 \\ 325 \\ 350 \end{array} \begin{array}{c} \begin{array}{ccccccccccc} 100 & 125 & 150 & 175 & 200 & 225 & 250 & 275 & 300 & 325 & 350 \end{array} \\ \left[\begin{array}{ccccccccccc} .669 & .180 & .099 & .039 & .011 & .002 & .000 & .000 & .000 & .000 & .000 \\ .450 & .231 & .176 & .095 & .036 & .010 & .002 & .000 & .000 & .000 & .000 \\ .246 & .218 & .229 & .171 & .091 & .034 & .009 & .002 & .000 & .000 & .000 \\ .106 & .151 & .220 & .228 & .167 & .086 & .032 & .008 & .002 & .000 & .000 \\ .035 & .077 & .156 & .223 & .226 & .162 & .082 & .030 & .008 & .001 & .000 \\ .009 & .029 & .081 & .161 & .225 & .223 & .157 & .078 & .028 & .007 & .001 \\ .002 & .008 & .031 & .085 & .165 & .227 & .221 & .152 & .074 & .026 & .008 \\ .000 & .002 & .009 & .033 & .090 & .170 & .229 & .218 & .148 & .071 & .031 \\ .000 & .000 & .002 & .010 & .036 & .094 & .175 & .231 & .215 & .143 & .095 \\ .000 & .000 & .000 & .002 & .010 & .038 & .098 & .179 & .232 & .212 & .227 \\ .000 & .000 & .000 & .000 & .002 & .011 & .041 & .103 & .184 & .233 & .426 \end{array}\right] \end{array}.$$

For North Creek, the transition matrices of the Markov chain in the normal, drought, and flood flow clusters, respectively, are

$$P_N^n = \begin{array}{c} \\ 20 \\ 45 \\ 70 \\ 95 \end{array} \begin{array}{c} \begin{array}{cccc} 20 & 45 & 70 & 95 \end{array} \\ \left[\begin{array}{cccc} .765 & .204 & .030 & .001 \\ .407 & .412 & .162 & .020 \\ .116 & .364 & .383 & .137 \\ .016 & .141 & .398 & .446 \end{array}\right] \end{array},$$

$$P_N^d = \begin{array}{c} \\ 5 \\ 30 \\ 55 \end{array} \begin{array}{c} \begin{array}{ccc} 5 & 30 & 55 \end{array} \\ \left[\begin{array}{ccc} .834 & .163 & .003 \\ .288 & .610 & .103 \\ .018 & .377 & .605 \end{array}\right] \end{array}, \text{ and}$$

$$P_N^f = \begin{array}{c} \\ 25 \\ 50 \\ 75 \\ 100 \\ 125 \\ 150 \\ 175 \\ 200 \end{array} \begin{array}{c} \begin{array}{cccccccc} 25 & 50 & 75 & 100 & 125 & 150 & 175 & 200 \end{array} \\ \left[\begin{array}{cccccccc} .670 & .211 & .091 & .023 & .004 & .000 & .000 & .000 \\ .408 & .287 & .200 & .082 & .020 & .003 & .000 & .000 \\ .182 & .252 & .284 & .188 & .074 & .017 & .002 & .000 \\ .057 & .144 & .261 & .279 & .176 & .066 & .015 & .002 \\ .012 & .053 & .156 & .268 & .273 & .165 & .059 & .014 \\ .002 & .013 & .060 & .167 & .275 & .267 & .153 & .063 \\ .000 & .002 & .015 & .068 & .179 & .280 & .259 & .197 \\ .000 & .000 & .002 & .018 & .076 & .191 & .284 & .428 \end{array}\right] \end{array}.$$

For our SDP, if the system moves to a different cluster in period t and the AR(1) process defined on the state space in period $t-1$ moves to a state in period t that is not in the state space in period t, we take the closest state in the state space in period t as the streamflow rate in period t.

For the electricity price, we consider the hourly average values of the real-time data available for New York City between the years 2007 and 2019; we retrieve this data from [41]. It is important to note that the electricity price can be negative according to our time series data. We model the hourly electricity prices as follows: First, we deseasonalize the price data to remove the effect of seasonal variation on our spike identification. Following Zhou et al. [25], we construct a seasonality model by fitting a linear regression to the price data:

$$s_t = \gamma_1 + \sum_{i=1}^{11} \gamma_{2i} D_t^{2i} + \sum_{j=1}^{6} \gamma_{3j} D_t^{3j} + \sum_{h=1}^{23} \gamma_{4h} D_t^{4h},$$

where γ_1 is a constant and γ_{2i}, γ_{3j}, and γ_{4h} are the coefficients of the dummy variables D_t^{2i}, D_t^{3j}, and D_t^{4h}, that are equal to one if period t is in month i, week day j, and hour h, respectively. Then, we remove the seasonal effect from the observed prices and determine the spikes under the assumption that the highest 5% and lowest 5% of the deseasonalized prices are outliers. The spikes are the differences between these outliers and the mean of the remaining deseasonalized prices after these outliers are removed. Fig. 4 illustrates the empirical distribution of the spikes. For a more refined seasonality model, we remove the spikes from the observed prices and fit the above linear regression to the despiked prices. Finally, we subtract the refined seasonal effect from the despiked prices and formulate the despiked and deseasonalized price, ρ_t, as an AR(1) process: $\rho_t = (1-\kappa)\rho_{t-1} + \sigma\epsilon_t$, $\forall t$, where κ is the speed of mean reversion and σ is the volatility of white noise. The parameter estimates of this AR(1) process are $\hat{\kappa} = 0.328$ and $\hat{\sigma} = 13.674$. Table 2 exhibits the parameter estimates of the seasonality model.

We employ the trinomial lattice method of Hull and White [42] to characterize the AR(1) process of the electricity price as a finite-state Markov chain. Following the suggestions of Hull and White [42] and Jaillet et al. [43] regarding the number of time steps that should be iterated, we construct a three-hour trinomial lattice for our AR(1) process (Fig. 5). The Markov chain obtained from this lattice has the state space $\mathcal{P} := \{-47.4, -23.7, 0, 23.7, 47.4\}$ and the following transition matrix:

$$P = \begin{array}{c} \\ -47.4 \\ -23.7 \\ 0.0 \\ 23.7 \\ 47.4 \end{array} \begin{array}{c} \begin{array}{ccccc} -47.4 & -23.7 & 0.0 & 23.7 & 47.4 \end{array} \\ \left[\begin{array}{ccccc} .398 & .548 & .056 & 0 & 0 \\ .056 & .559 & .384 & 0 & 0 \\ 0 & .167 & .667 & .167 & 0 \\ 0 & 0 & .384 & .559 & .056 \\ 0 & 0 & .054 & .548 & .398 \end{array}\right] \end{array}.$$

We also restrict the spikes to take values from the set $\mathcal{J} := \{-500, -400, \ldots, 1200, 1300\}$. Note that the spike occurrence probability is 10% in each period.

For our numerical study, we construct twelve different scenarios in which the pumping capability is turned on (PHES) or off (CCHS); the upper reservoir is fed by the Hudson River at Fort Edward or at North Creek; and the planning horizon spans the month of January, April, or August in 2019 ($T = 720$ h). We employ the efficiency curve of Francis turbines [44] for our efficiency calculations; the same curve applies to the upper and lower turbines in the discharging mode as well as the pump (turbine in reverse mode) in the charging mode (we do not require Assumption 1 in our experiments). We assume that $h_1 = h_2 = 100\ m$, $C_U = C_L = 10\ hm^3$, $Q_{RU} = Q_{RL} = Q_P = 0.4\ hm^3$, and $x_{u1} = x_{l1} = 5\ hm^3$ for our base case; we conduct our experiments by varying the values of C_U, C_L, h_1, h_2, and negative price occurrence frequency (NPF). The NPF is 4.90% in January, 6.76% in April, and 6.76% in August, according to our price model. For each month, we obtain two other values of NPF (in addition to the one observed in our price model) by multiplying the numbers of negative spike occurrences in our price model with certain constants. The initial exogenous states for Fort Edward and North Creek are $y_1 = (150, 0)$ and $y_1 = (45, 0)$ in January, $y_1 = (225, 0)$ and $y_1 = (100, 0)$ in April, and $y_1 = (125, 0)$ and $y_1 = (30, 0)$ in August, respectively. Finally, x_{ut} and x_{lt} take values from the set $\{0, 0.2, 0.4, \ldots, 10\}$, a_t takes values from the set $\{-0.4, -0.2, 0, 0.2, 0.4\}$, and b_t takes values from the set $\{0, 0.2, 0.4\}$. We solve the recursion of our SDP in each instance, with Figs. 6 and 7 showing our results.

3.3. Discussion of the numerical results

We observe from Fig. 6 that, for both system configurations at Fort Edward, the total cash flow (TCF) decreases as the NPF grows, with the exception of the PHES system in August. However, in contrast to the CCHS, the PHES system is expected to benefit from an increase in the NPF. This counter-intuitive result can be explained by the availability of excess streamflow in January and April that dampens the incentive to pump water to purchase energy at low prices. The PHES system operator considers purchasing energy at only negative prices in January and April, leading to relatively small amounts of energy purchased from the market. Consequently, in the months of January and April with high streamflow rates, both system configurations yield similar and large amounts of water released from both reservoirs as well as energy sold to the market, thereby suffering from an increase in the NPF. Motivated by our observation in August with low streamflow rate, we repeat our experiments for North Creek with much lower streamflow rates compared to Fort Edward. We observe that the lower streamflow availability significantly drains the TCF for both system configurations, and the PHES system at North Creek always benefits from an increase in the NPF. The PHES transformation provides the greatest benefit (with

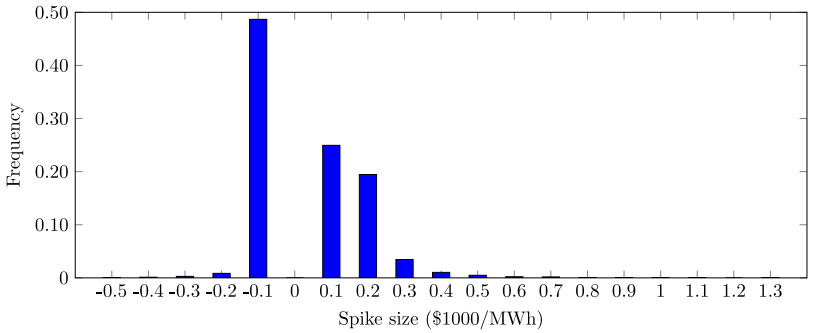

Fig. 4. Empirical distribution of the spikes.

Table 2
Parameter estimates of the despiked price seasonality model.

$\hat{\gamma}_1$	34.50											
i	1	2	3	4	5	6	7	8	9	10	11	
$\hat{\gamma}_{2i}$	19.3	13.1	−1.5	−6.5	−9.5	−10.2	−5.5	−6.4	−9.0	−10.0	−6.4	
j	1	2	3	4	5	6						
$\hat{\gamma}_{3j}$	4.1	4.2	4.5	4.3	3.7	1.6						
h	1	2	3	4	5	6	7	8	9	10	11	12
$\hat{\gamma}_{4h}$	−1.9	−3.7	−3.4	−2.8	−1.6	2.6	5.0	7.3	9.4	10.5	10.4	10.4
h	13	14	15	16	17	18	19	20	21	22	23	
$\hat{\gamma}_{4h}$	9.6	9.0	9.3	11.6	15.4	15.6	13.2	9.9	6.4	3.0	0.6	

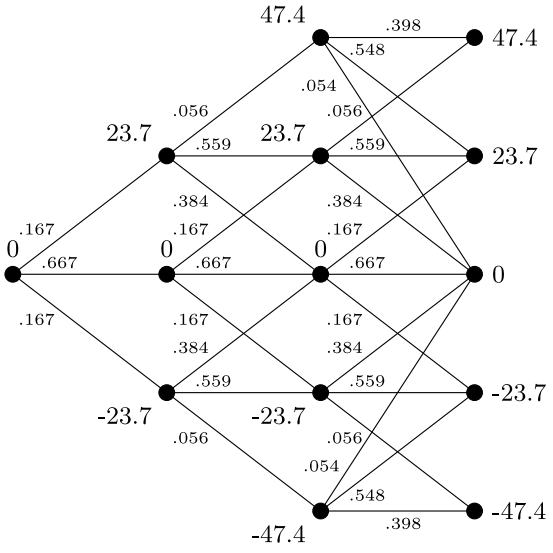

Fig. 5. Trinomial lattice for the despiked and deseasonalized price. Nodes represent discrete states of the Markov chain and arcs represent transitions between these states.

an improvement of 59.2% in the TCF) at North Creek in August when the NPF is highest.

For both Fort Edward and North Creek, our time series models indicate that the streamflow rates are the highest in April and the lowest in August, while the electricity prices are the highest in January and the lowest in April. For Fort Edward, the price effect is more dominant so that the amounts of energy sold and the TCFs are the highest in January. For North Creek, on the other hand, the streamflow effect is more dominant so that the amounts of energy sold are the highest in April. However, since the electricity price in January is significantly higher than in April, the large amounts of energy sold in April cannot lead to higher TCFs in April than in January.

We observe from Fig. 7 that the PHES transformation tends to become more beneficial as the capacity levels of the upper and lower reservoirs grow only up to certain points. This increase in the value of PHES is more significant at North Creek in August. We also note that the benefit of PHES transformation increases as the head of the upper station increases, while it decreases as the head of the lower station increases. This is because increasing the head of the upper station improves the pumping capability of the PHES system, whereas increasing the head of the lower station improves the energy generation potential in the lower reservoir, reducing the need for energy storage by pumping water. This change in the value of PHES is again more significant at North Creek in August.

The tightness of our upper bound in Theorem 1 is greatly influenced by the range in which the electricity prices vary. Our upper bound may not be tight enough in markets with high price spikes, particularly when the negative prices exist within the volatile structure. The price range is high in our experiments: In January, the maximum and minimum prices are $300.99 and −$62.7 per MWh, respectively, leading to an upper bound of 26 million dollars. In April, the maximum and minimum prices are $379.76 and −$79.41 per MWh, respectively, leading to an upper bound of 33 million dollars. In August, the maximum and minimum prices are $163.91 and −$6.4 per MWh, respectively, leading to an upper bound of 12 million dollars. Our upper bound is thus noticeably tighter at North Creek in August, when the PHES transformation provides the greatest benefit due to the limited streamflow availability. Our upper bound is expected to be much tighter in more stable markets like Nord Pool. For instance, Norway experienced low price ranges with the maximum and minimum prices of (€68.00, €43.81), (€60.70, €27.91), and (€52.79, €28.96) per MWh, in January, April, and August of 2019, respectively [45].

4. Comparison with deterministic solution approach

We compare our solution approach with a deterministic one and measure the value of including randomness in our formulation. The advantage of using a stochastic solution over a deterministic solution, i.e., the value of the stochastic solution (VSS), determines the cost of ignoring uncertainty in decision-making. Concentrating on the despiked prices in this section, we consider the deterministic version of our problem that ignores uncertainty by replacing the random components (r_t for the streamflow rate and ρ_t for the electricity price) with their expected values. Let π^d denote the optimal policy for this deterministic

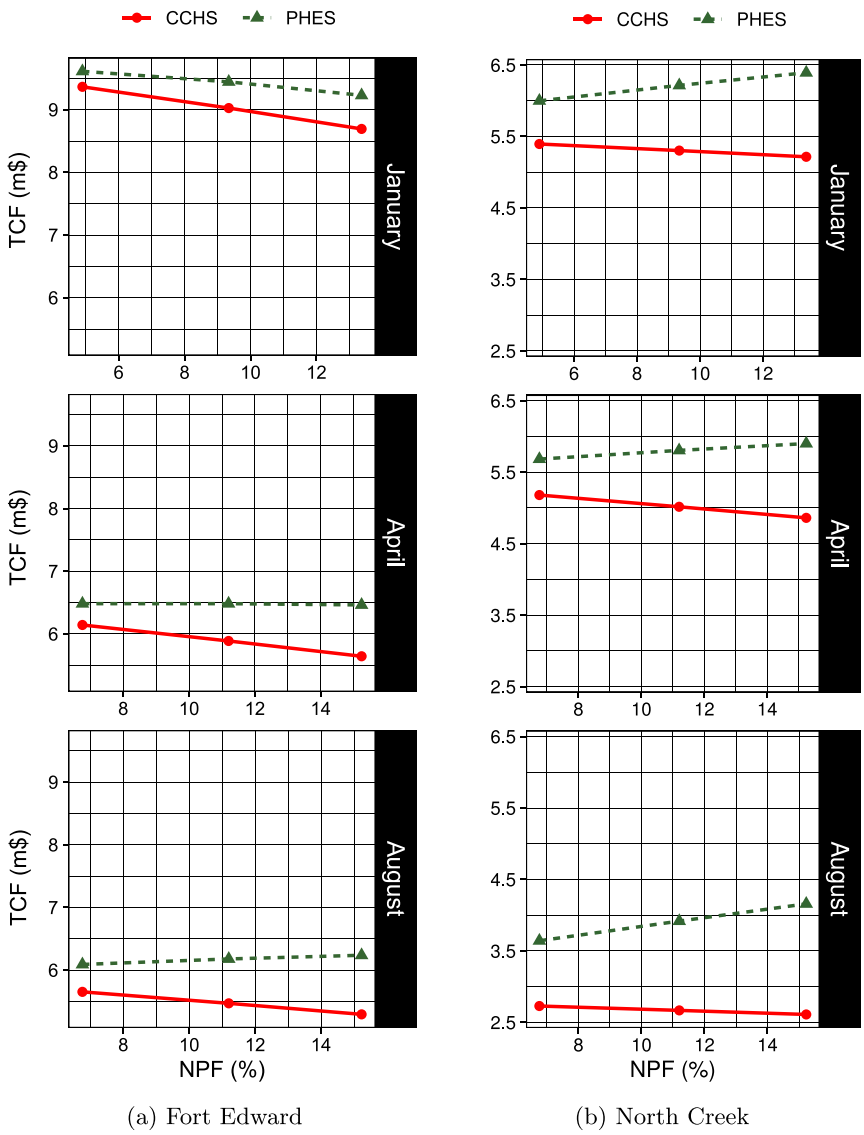

(a) Fort Edward (b) North Creek

Fig. 6. Numerical results for the value of PHES with respect to NPF.

Table 3
Numerical results for the VSS.

Type	Season	Fort Edward			North Creek		
		S	D	VSS (%)	S	D	VSS (%)
CCHS	January	8.473	8.221	2.97	4.314	3.812	11.64
	April	5.157	4.954	3.94	4.133	3.771	8.76
	August	4.607	4.253	8.07	1.704	1.334	21.71
PHES	January	8.490	8.230	3.06	4.555	3.890	14.60
	April	5.199	4.983	4.15	4.303	3.846	10.62
	August	4.724	4.305	8.87	2.199	1.521	30.83

S: TCF of the optimal policy. D: TCF of the policy π^d.

problem. The TCF of the policy π^d can be calculated from the recursion in (5) (without optimization) when the actions are restricted to obey the policy π^d in each state and each period. Table 3 exhibits the VSS (i.e., the percentage improvement in the TCF via the stochastic solution) for the base case in each of our twelve scenarios. We have found that the VSS is maximum at North Creek in August (21.71% and 30.83% for CCHS and PHES, respectively).

5. Conclusions

We consider a CCHS that can be converted to a PHES system by utilizing a reversible turbine between the reservoirs. In order to examine the value of this transformation, we formulate the energy generation and storage problem in both systems as an SDP by taking into account uncertainties in the streamflow rate and electricity price. With this formulation, we analytically derive an upper bound on the profit improvement that can be obtained from this transformation. Using data-calibrated time series models for the streamflow rate and electricity price, we solve the problem to optimality for various realistic cases of these systems in different seasons. Our numerical results imply that PHES becomes an important large scale storage option when the negative prices occur more frequently or the streamflow availability is more limited. Although adding a reversible turbine to a CCHS to obtain a PHES system can significantly increase the profits, a cost–benefit analysis is required in real-life cases to compare the cost of transformation with the profit improvement. Our SDP can help policymakers and investors to calculate the benefit in such an analysis, accurately taking into account the problem's stochastic and nonlinear nature. Future research may extend our analysis to hydropower stations integrated

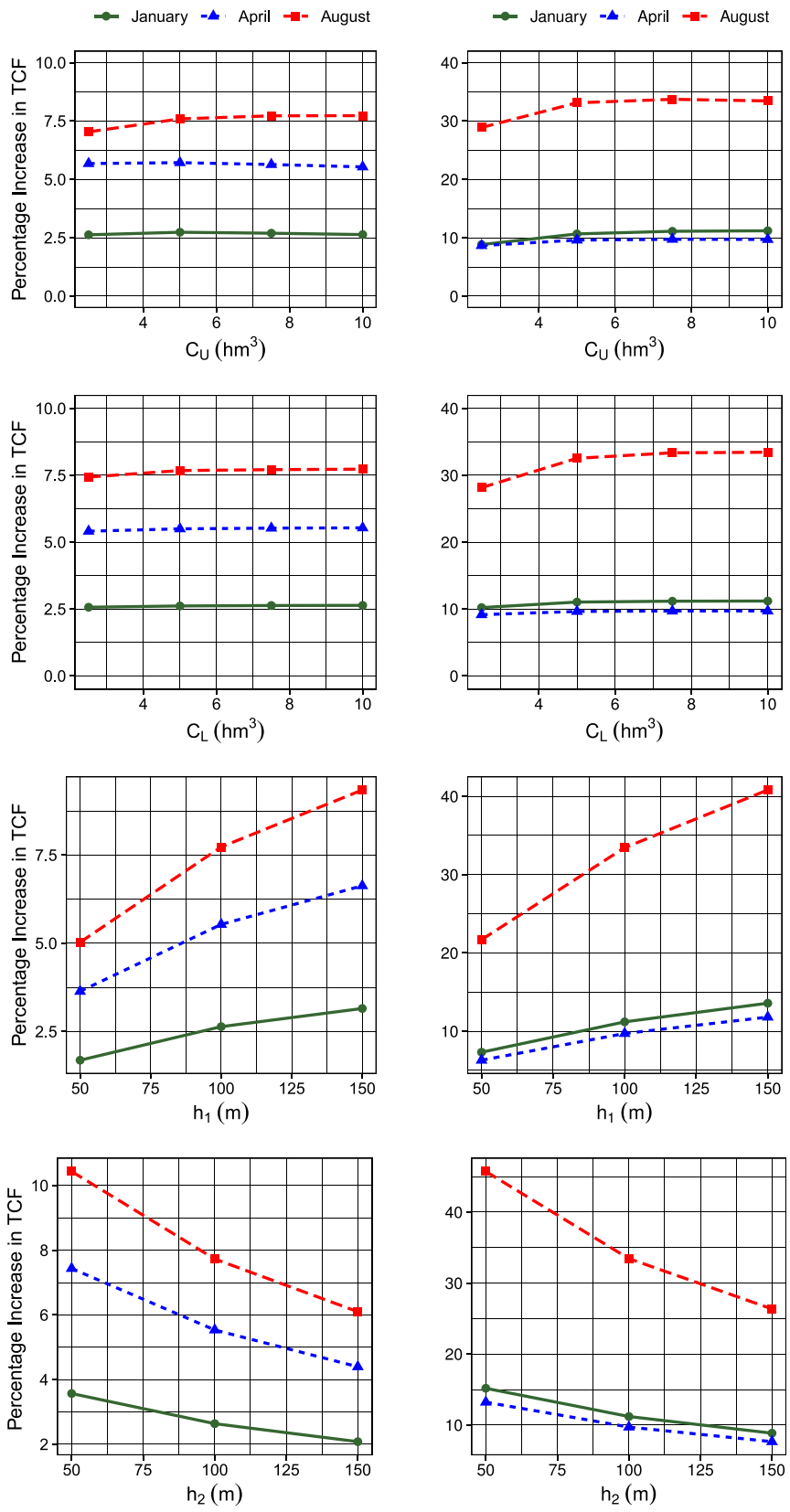

(a) Fort Edward (b) North Creek

Fig. 7. Numerical results for the value of PHES with respect to physical system characteristics.

with other renewable energy sources (e.g., solar and wind). Future extensions may also investigate the benefit of PHES transformation in different market settings, such as forward markets that enforce electricity trading through commitments submitted by participants.

CRediT authorship contribution statement

Parinaz Toufani: Conceptualization, Methodology, Formal analysis, Software, Investigation, Writing – original draft. **Emre Nadar:** Conceptualization, Methodology, Formal analysis, Writing – original draft, Supervision. **Ayse Selin Kocaman:** Conceptualization, Methodology, Formal analysis, Writing – original draft, Supervision.

Declaration of competing interest

The authors declare that they have no known competing financial interests or personal relationships that could have appeared to influence the work reported in this paper.

Acknowledgments

The authors thank the editors and three anonymous referees for their constructive comments and suggestions. We also thank Harun Avci, Northwestern University, for his valuable feedback during the numerical analysis stage of our work. This research has been supported by the Scientific and Technological Research Council of Turkey (TÜBİTAK) [Grant 121M138]. Dr. Kocaman was supported by the BAGEP Award of the Science Academy, Turkey.

Appendix. Proof of Theorem 1

First, we will prove that $\widetilde{v}_t^*(x_{ut},x_{lt},y_t) \le v_t^*(x_{ut},x_{lt},y_t),\ \forall t\in\mathcal{T}$. Note that $\widetilde{v}_T^*(x_{uT},x_{lT},y_T)=v_T^*(x_{uT},x_{lT},y_T)=0$. Assuming $\widetilde{v}_{t+1}^*(x_{u(t+1)},x_{l(t+1)},y_{t+1}) \le v_{t+1}^*(x_{u(t+1)},x_{l(t+1)},y_{t+1})$, we show $\widetilde{v}_t^*(x_{ut},x_{lt},y_t)\le v_t^*(x_{ut},x_{lt},y_t)$. Let $\widetilde{a}=\widetilde{a}_t^*(x_{ut},x_{lt},y_t)\ge 0$ and $\widetilde{b}=\widetilde{b}_t^*(x_{ut},x_{lt},y_t)$ denote the optimal actions in state (x_{ut},x_{lt},y_t) for the CCHS. Also, let $\widetilde{\mathbb{U}}(x_{ut},x_{lt},y_t)$ denote the set of admissible action pairs (a_t,b_t) in state (x_{ut},x_{lt},y_t) for the CCHS. Since $\widetilde{\mathbb{U}}(x_{ut},x_{lt},y_t)\subseteq\mathbb{U}(x_{ut},x_{lt},y_t)$, $(\widetilde{a},\widetilde{b})\in\mathbb{U}(x_{ut},x_{lt},y_t)$. Thus:

$$
\begin{aligned}
&\widetilde{v}_t^*(x_{ut},x_{lt},y_t)\\
&= R(\widetilde{a},\widetilde{b},y_t)+\mathbb{E}\Big[\,\widetilde{v}_{t+1}^*\big(\min\{x_{ut}-\widetilde{a}+r_{t+1},C_U\},\\
&\quad \min\big\{\min\{x_{lt}+\widetilde{a},C_L\}-\widetilde{b}+(x_{ut}-\widetilde{a}-C_U+r_{t+1})^+,C_L\big\},y_{t+1}\big)\,\Big]\\
&\le R(\widetilde{a},\widetilde{b},y_t)+\mathbb{E}\Big[\,v_{t+1}^*\,\big(\,\min\big\{x_{ut}-\widetilde{a}+r_{t+1},C_U\big\},\min\{\min\{x_{lt}+\widetilde{a},C_L\}\\
&\quad -\widetilde{b}+(x_{ut}-\widetilde{a}-C_U+r_{t+1})^+,C_L\},y_{t+1}\,\big)\Big]\le v_t^*(x_{ut},x_{lt},y_t).
\end{aligned}
$$

Next, we will prove that:

$$
v_t^*(x_{ut},x_{lt},y_t) \le \widetilde{v}_t^*(x_{ut},x_{lt},y_t)+Q_P\rho g h_1(T-t)\left(\phi_{RU}\max_{t\le\tau\le T}\overline{p}_\tau-\min_{t\le\tau\le T}\underline{p}_\tau/\phi_P\right)^+,\ \forall t\in\mathcal{T}.
$$

Note that $v_T^*(x_{uT},x_{lT},y_T)=\widetilde{v}_T^*(x_{uT},x_{lT},y_T)+Q_P\rho g h_1(T-T)(\phi_{RU}\overline{p}_T-\underline{p}_T/\phi_P)^+=0$. To this end, we first show that $\widetilde{v}_t^*(x_{ut},x_{lt},y_t)-\widetilde{v}_t^*(x_{ut}-\alpha,x_{lt}+\alpha,y_t)\le\rho g h_1\alpha\phi_{RU}\max_{t\le\tau\le T}\overline{p}_\tau$ where $0\le\alpha\le\min\{x_{ut},C_L-x_{lt}\},\ \forall t\in\mathcal{T}$. Note that $\widetilde{v}_T^*(x_{uT},x_{lT},y_T)=\widetilde{v}_T^*(x_{uT}-\alpha,x_{lT}+\alpha,y_T)=0$. Assuming $\widetilde{v}_{t+1}^*(x_{u(t+1)},x_{l(t+1)},y_{(t+1)})-\widetilde{v}_{t+1}^*(x_{u(t+1)}-\alpha,x_{l(t+1)}+\alpha,y_{(t+1)})\le\rho g h_1\alpha\phi_{RU}\max_{t+1\le\tau\le T}\overline{p}_\tau$, we show $\widetilde{v}_t^*(x_{ut},x_{lt},y_t)-\widetilde{v}_t^*(x_{ut}-\alpha,x_{lt}+\alpha,y_t)\le\rho g h_1\alpha\phi_{RU}\max_{t\le\tau\le T}\overline{p}_\tau$. Suppose that $\widetilde{a}=\widetilde{a}_t^*(x_{ut},x_{lt},y_t)\ge\alpha$. Recall that $\widetilde{b}=\widetilde{b}_t^*(x_{ut},x_{lt},y_t)$. Notice that $(\widetilde{a}-\alpha,\widetilde{b})\in\widetilde{\mathbb{U}}(x_{ut}-\alpha,x_{lt}+\alpha,y_t)$. Thus:

$$
\begin{aligned}
&\widetilde{v}_t^*(x_{ut},x_{lt},y_t)-\widetilde{v}_t^*(x_{ut}-\alpha,x_{lt}+\alpha,y_t)\\
&\le R(\widetilde{a},\widetilde{b},y_t)+\mathbb{E}\Big[\widetilde{v}_{t+1}^*\big(\min\{x_{ut}-\widetilde{a}+r_{t+1},C_U\},\\
&\quad \min\{\min\{x_{lt}+\widetilde{a},C_L\}-\widetilde{b}+(x_{ut}-\widetilde{a}-C_U+r_{t+1})^+,\\
&\quad C_L\},y_{(t+1)}\big)\Big]-R(\widetilde{a}-\alpha,\widetilde{b},y_t)\\
&\quad -\mathbb{E}\Big[\widetilde{v}_{t+1}^*\big(\min\{x_{ut}-\alpha-(\widetilde{a}-\alpha)+r_{t+1},C_U\},\\
&\quad \min\{\min\{x_{lt}+\alpha+(\widetilde{a}-\alpha),C_L\}-\widetilde{b}\\
&\quad +\big(x_{ut}-\alpha-(\widetilde{a}-\alpha)-C_U+r_{t+1}\big)^+,C_L\},y_{(t+1)}\big)\Big]\\
&= p_t\rho g h_1\phi_{RU}(\widetilde{a}-\widetilde{a}+\alpha)+p_t\rho g h_2\phi_{RL}(\widetilde{b}-\widetilde{b})\\
&\le \rho g h_1\alpha\phi_{RU}\max_{t\le\tau\le T}\overline{p}_\tau.
\end{aligned}
$$

Now suppose that $\widetilde{a}<\alpha$. If the optimal actions $(\widetilde{a},\widetilde{b})$ are taken in state (x_{ut},x_{lt},y_t):

$$
\begin{aligned}
&x_{u(t+1)}=\min\{x_{ut}-\widetilde{a}+r_{t+1},C_U\}\ \text{and}\\
&x_{l(t+1)}=\min\{x_{lt}+\widetilde{a}-\widetilde{b}+(x_{ut}-\widetilde{a}-C_U+r_{t+1})^+,C_L\}.
\end{aligned}
$$

If the actions $(0,\widetilde{b})$ are taken in state $(x_{ut}-\alpha,x_{lt}+\alpha,y_t)$:

$$
\begin{aligned}
&x'_{u(t+1)}=\min\{x_{ut}-\alpha+r_{t+1},C_U\}\ \text{and}\\
&x'_{l(t+1)}=\min\{x_{lt}+\alpha-\widetilde{b}+(x_{ut}-\alpha-C_U+r_{t+1})^+,C_L\}.
\end{aligned}
$$

For these state variables, we make the following observations:

(1) If $x_{ut}-\widetilde{a}+r_{t+1}\le C_U$, $x'_{u(t+1)}=x_{ut}-\alpha+r_{t+1}=x_{u(t+1)}-(\alpha-\widetilde{a})$ and $x'_{l(t+1)}=x_{lt}+\alpha-\widetilde{b}=x_{l(t+1)}+(\alpha-\widetilde{a})$.
(2) If $x_{ut}-\alpha+r_{t+1}\le C_U\le x_{ut}-\widetilde{a}+r_{t+1}$ and $x_{ut}+x_{lt}-\widetilde{b}-C_U+r_{t+1}\le C_L$, $x'_{u(t+1)}=x_{ut}-\alpha+r_{t+1}=x_{u(t+1)}-(C_U-r_{t+1}-x_{ut}+\alpha)$ and $x'_{l(t+1)}=x_{lt}+\alpha-\widetilde{b}=x_{l(t+1)}+(C_U-r_{t+1}-x_{ut}+\alpha)$. Note that $0\le C_U-r_{t+1}-x_{ut}+\alpha\le\alpha-\widetilde{a}$.
(3) If $x_{ut}-\alpha+r_{t+1}\le C_U\le x_{ut}-\widetilde{a}+r_{t+1}$ and $x_{ut}+x_{lt}-\widetilde{b}-C_U+r_{t+1}>C_L$, note that $x_{lt}+\alpha-\widetilde{b}>C_L$. This scenario is not possible since $x_{lt}+\alpha\le C_L$.
(4) If $C_U\le x_{ut}-\alpha+r_{t+1}$, $x'_{u(t+1)}=x_{u(t+1)}=C_U$ and $x'_{l(t+1)}=x_{l(t+1)}=\min\{x_{lt}-\widetilde{b}+x_{ut}-C_U+r_{t+1},C_L\}$.

Thus, there exists β such that $0\le\beta\le\alpha-\widetilde{a}$ and

$$
\begin{aligned}
&\widetilde{v}_t^*(x_{ut},x_{lt},y_t)-\widetilde{v}_t^*(x_{ut}-\alpha,x_{lt}+\alpha,y_t)\\
&\le R(\widetilde{a},\widetilde{b},y_t)+\mathbb{E}\Big[\widetilde{v}_{t+1}^*\big(x_{u(t+1)},x_{l(t+1)},y_{(t+1)}\big)\Big]\\
&\quad -R(0,\widetilde{b},y_t)-\mathbb{E}\Big[\widetilde{v}_{t+1}^*\big(x'_{u(t+1)},x'_{l(t+1)},y_{(t+1)}\big)\Big]\\
&= p_t\rho g h_1\phi_{RU}\widetilde{a}+\mathbb{E}\Big[\widetilde{v}_{t+1}^*\big(x_{u(t+1)},x_{l(t+1)},y_{(t+1)}\big)\Big]\\
&\quad -\mathbb{E}\Big[\widetilde{v}_{t+1}^*\big(x_{u(t+1)}-\beta,x_{l(t+1)}+\beta,y_{(t+1)}\big)\Big]\\
&\le \widetilde{a}\rho g h_1\phi_{RU}p_t+\beta\rho g h_1\phi_{RU}\max_{t+1\le\tau\le T}\overline{p}_\tau\\
&\le \widetilde{a}\rho g h_1\phi_{RU}\max_{t\le\tau\le T}\overline{p}_\tau+\beta\rho g h_1\phi_{RU}\max_{t\le\tau\le T}\overline{p}_\tau\\
&\le \alpha\rho g h_1\phi_{RU}\max_{t\le\tau\le T}\overline{p}_\tau.
\end{aligned}
$$

Using the above result and assuming $v_{t+1}^*(x_{u(t+1)},x_{l(t+1)},y_{(t+1)})-\widetilde{v}_{t+1}^*(x_{u(t+1)},x_{l(t+1)},y_{(t+1)})\le Q_P\rho g h_1(T-t-1)\left(\phi_{RU}\max_{t+1\le\tau\le T}\overline{p}_\tau-\min_{t+1\le\tau\le T}\underline{p}_\tau/\phi_P\right)^+$, we show $v_t^*(x_{ut},x_{lt},y_t)-\widetilde{v}_t^*(x_{ut},x_{lt},y_t)\le Q_P\rho g h_1(T-t)\left(\phi_{RU}\max_{t\le\tau\le T}\overline{p}_\tau-\min_{t\le\tau\le T}\underline{p}_\tau/\phi_P\right)^+$. Let $a=a^*(x_{ut},x_{lt},y_t)$ and $b=b^*(x_{ut},x_{lt},y_t)$ denote the optimal actions in state (x_{ut},x_{lt},y_t) for the PHES system. Suppose that $a\ge 0$. Note $(a,b)\in\widetilde{\mathbb{U}}(x_{ut},x_{lt},y_t)$. Thus:

$$
\begin{aligned}
&v_t^*(x_{ut},x_{lt},y_t)-\widetilde{v}_t^*(x_{ut},x_{lt},y_t)\\
&\le R(a,b,y_t)+\mathbb{E}\Big[v_{t+1}^*\big(\min\{x_{ut}-a+r_{t+1},C_U\},\\
&\quad \min\{\min\{x_{lt}+a,C_L\}-b+(x_{ut}-a-C_U+r_{t+1})^+,\\
&\quad C_L\},y_{(t+1)}\big)\Big]-R(a,b,y_t)-\mathbb{E}\Big[\widetilde{v}_{t+1}^*\big(\min\{x_{ut}-a+r_{t+1},C_U\},\\
&\quad \min\{\min\{x_{lt}+a,C_L\}-b+(x_{ut}-a-C_U+r_{t+1})^+,C_L\},y_{(t+1)}\big)\Big]\\
&\le Q_P\rho g h_1(T-t-1)\left(\phi_{RU}\max_{t+1\le\tau\le T}\overline{p}_\tau-\min_{t+1\le\tau\le T}\underline{p}_\tau/\phi_P\right)^+
\end{aligned}
$$

$$\leq Q_P \rho g h_1 (T-t) \left(\phi_{RU} \max_{t \leq \tau \leq T} \overline{p}_\tau - \min_{t \leq \tau \leq T} \underline{p}_\tau / \phi_P \right)^+ .$$

Now suppose that $a < 0$. Note that $b = 0$ in this case. If the optimal actions $(a, 0)$ are taken in state (x_{ut}, x_{lt}, y_t) for the PHES system:

$$x_{u(t+1)} = \min\{x_{ut} - a + r_{t+1}, C_U\} \text{ and}$$
$$x_{l(t+1)} = \min \Big\{ x_{lt} + a + \left(x_{ut} - a - C_U\right)^+ + \left(\min\{x_{ut} - a, C_U\} + r_{t+1} - C_U\right)^+, C_L \Big\}.$$

If the actions $(0, 0)$ are taken in state (x_{ut}, x_{lt}, y_t) for the CCHS:

$$x'_{u(t+1)} = \min\{x_{ut} + r_{t+1}, C_U\} \text{ and}$$
$$x'_{l(t+1)} = \min\left\{x_{lt} + \left(x_{ut} + r_{t+1} - C_U\right)^+, C_L\right\}.$$

For these state variables, we make the following observations:

(1) If $x_{ut} - a + r_{t+1} \leq C_U$, $x'_{u(t+1)} = x_{ut} + r_{t+1} = x_{u(t+1)} - (-a)$ and $x'_{l(t+1)} = x_{lt} = x_{l(t+1)} + (-a)$.
(2) If $\max\{x_{ut} + r_{t+1}, x_{ut} - a\} \leq C_U \leq x_{ut} - a + r_{t+1}$, $x'_{u(t+1)} = x_{ut} + r_{t+1} = x_{u(t+1)} - (C_U - r_{t+1} - x_{ut})$ and $x'_{l(t+1)} = x_{lt} = x_{l(t+1)} + (C_U - r_{t+1} - x_{ut})$. Note that $0 \leq C_U - r_{t+1} - x_{ut} \leq -a$.
(3) If $x_{ut} - a \leq C_U \leq x_{ut} + r_{t+1}$ and $x_{ut} + x_{lt} + r_{t+1} - C_U \leq C_L$, $x'_{u(t+1)} = x_{u(t+1)} = C_U$ and $x'_{l(t+1)} = x_{l(t+1)} = x_{ut} + x_{lt} + r_{t+1} - C_U$.
(4) If $x_{ut} - a \leq C_U \leq x_{ut} + r_{t+1}$ and $x_{ut} + x_{lt} + r_{t+1} - C_U > C_L$, $x'_{u(t+1)} = x_{u(t+1)} = C_U$ and $x'_{l(t+1)} = x_{l(t+1)} = C_L$.
(5) If $x_{ut} + r_{t+1} \leq C_U \leq x_{ut} - a$, $x'_{u(t+1)} = x_{ut} + r_{t+1} = x_{u(t+1)} - (C_U - r_{t+1} - x_{ut})$ and $x'_{l(t+1)} = x_{lt} = x_{l(t+1)} + (C_U - r_{t+1} - x_{ut})$. Note that $0 \leq C_U - r_{t+1} - x_{ut} \leq -a$.
(6) If $C_U \leq \min\{x_{ut} - a, x_{ut} + r_{t+1}\}$ and $x_{ut} + x_{lt} + r_{t+1} - C_U \leq C_L$, $x'_{u(t+1)} = x_{u(t+1)} = C_U$ and $x'_{l(t+1)} = x_{l(t+1)} = x_{ut} + x_{lt} + r_{t+1} - C_U$.
(7) If $C_U \leq \min\{x_{ut} - a, x_{ut} + r_{t+1}\}$ and $x_{ut} + x_{lt} + r_{t+1} - C_U > C_L$, $x'_{u(t+1)} = x_{u(t+1)} = C_U$ and $x'_{l(t+1)} = x_{l(t+1)} = C_L$.

Thus, there exists α such that $0 \leq \alpha \leq -a$ and

$$\begin{aligned}
&v_t^*(x_{ut}, x_{lt}, y_t) - \widetilde{v}_t^*(x_{ut}, x_{lt}, y_t) \\
&\leq R(a, 0, y_t) + \mathbb{E}\left[v_{t+1}^*\left(x_{u(t+1)}, x_{l(t+1)}, y_{(t+1)}\right)\right] \\
&\quad - R(0, 0, y_t) - \mathbb{E}\left[\widetilde{v}_{t+1}^*\left(x'_{u(t+1)}, x'_{l(t+1)}, y_{(t+1)}\right)\right] \\
&= p_t a \rho g h_1 / \phi_P + \mathbb{E}\left[v_{t+1}^*\left(x_{u(t+1)}, x_{l(t+1)}, y_{(t+1)}\right)\right. \\
&\quad \left. - \widetilde{v}_{t+1}^*\left(x_{u(t+1)} - \alpha, x_{l(t+1)} + \alpha, y_{(t+1)}\right)\right] \\
&\leq p_t a \rho g h_1 / \phi_P + \mathbb{E}\left[v_{t+1}^*\left(x_{u(t+1)}, x_{l(t+1)}, y_{(t+1)}\right)\right. \\
&\quad \left. - \widetilde{v}_{t+1}^*\left(x_{u(t+1)}, x_{l(t+1)}, y_{(t+1)}\right)\right] + \alpha \rho g h_1 \phi_{RU} \max_{t+1 \leq \tau \leq T} \overline{p}_\tau \\
&\leq p_t a \rho g h_1 / \phi_P + \alpha \rho g h_1 \phi_{RU} \max_{t+1 \leq \tau \leq T} \overline{p}_\tau \\
&\quad + Q_P \rho g h_1 (T - t - 1) \left(\phi_{RU} \max_{t+1 \leq \tau \leq T} \overline{p}_\tau - \min_{t+1 \leq \tau \leq T} \underline{p}_\tau / \phi_P \right)^+ .
\end{aligned}$$

If $p_t \geq 0$:

$$\begin{aligned}
&p_t a \rho g h_1 / \phi_P + \alpha \rho g h_1 \phi_{RU} \max_{t+1 \leq \tau \leq T} \overline{p}_\tau \\
&\leq -p_t \alpha \rho g h_1 / \phi_P + \alpha \rho g h_1 \phi_{RU} \max_{t+1 \leq \tau \leq T} \overline{p}_\tau \\
&\leq -\alpha \rho g h_1 / \phi_P \min_{t \leq \tau \leq T} \underline{p}_\tau + \alpha \rho g h_1 \phi_{RU} \max_{t \leq \tau \leq T} \overline{p}_\tau \\
&\leq \alpha \rho g h_1 \left(\phi_{RU} \max_{t \leq \tau \leq T} \overline{p}_\tau - \min_{t \leq \tau \leq T} \underline{p}_\tau / \phi_P \right)^+ \\
&\leq Q_P \rho g h_1 \left(\phi_{RU} \max_{t \leq \tau \leq T} \overline{p}_\tau - \min_{t \leq \tau \leq T} \underline{p}_\tau / \phi_P \right)^+ .
\end{aligned}$$

If $p_t < 0$:

$$\begin{aligned}
&p_t a \rho g h_1 / \phi_P + \alpha \rho g h_1 \phi_{RU} \max_{t+1 \leq \tau \leq T} \overline{p}_\tau \\
&\leq -Q_P \rho g h_1 p_t / \phi_P + \alpha \rho g h_1 \phi_{RU} \max_{t+1 \leq \tau \leq T} \overline{p}_\tau \\
&\leq -Q_P \rho g h_1 / \phi_P \min_{t \leq \tau \leq T} \underline{p}_\tau + Q_P \rho g h_1 \phi_{RU} \max_{t \leq \tau \leq T} \overline{p}_\tau \\
&\leq Q_P \rho g h_1 \left(\phi_{RU} \max_{t \leq \tau \leq T} \overline{p}_\tau - \min_{t \leq \tau \leq T} \underline{p}_\tau / \phi_P \right)^+ .
\end{aligned}$$

Thus,

$$\begin{aligned}
&v_t^*(x_{ut}, x_{lt}, y_t) - \widetilde{v}_t^*(x_{ut}, x_{lt}, y_t) \\
&\leq Q_P \rho g h_1 \left(\phi_{RU} \max_{t \leq \tau \leq T} \overline{p}_\tau - \min_{t \leq \tau \leq T} \underline{p}_\tau / \phi_P \right)^+ \\
&\quad + Q_P \rho g h_1 (T - t - 1) \left(\phi_{RU} \max_{t+1 \leq \tau \leq T} \overline{p}_\tau - \min_{t+1 \leq \tau \leq T} \underline{p}_\tau / \phi_P \right)^+ \\
&\leq Q_P \rho g h_1 (T - t) \left(\phi_{RU} \max_{t \leq \tau \leq T} \overline{p}_\tau - \min_{t \leq \tau \leq T} \underline{p}_\tau / \phi_P \right)^+ .
\end{aligned}$$

References

[1] R. Amirante, E. Cassone, E. Distaso, P. Tamburrano, Overview on recent developments in energy storage: Mechanical, electrochemical and hydrogen technologies, Energy Convers. Manage. 132 (2017) 372–387.
[2] B.S. Pali, S. Vadhera, An innovative continuous power generation system comprising of wind energy along with pumped-hydro storage and open well, IEEE Trans. Sustain. Energy (2018).
[3] I.A.G. Wilson, E. Barbour, T. Ketelaer, W. Kuckshinrichs, An analysis of storage revenues from the time-shifting of electrical energy in Germany and Great Britain from 2010 to 2016, J. Energy Storage 17 (2018) 446–456.
[4] IRENA, Innovative Operation of Pumped Hydropower Storage, Technical Report, International Renewable Energy Agency, Abu Dhabi, 2020.
[5] M.H. Ali, B. Wu, R.A. Dougal, An overview of SMES applications in power and energy systems, IEEE Trans. Sustain. Energy 1 (1) (2010) 38–47.
[6] S. Kucukali, Finding the most suitable existing hydropower reservoirs for the development of pumped-storage schemes: An integrated approach, Renew. Sustain. Energy Rev. 37 (2014) 502–508.
[7] P.D. Brown, J.A.P. Lopes, M.A. Matos, Optimization of pumped storage capacity in an isolated power system with large renewable penetration, IEEE Trans. Power Syst. 23 (2) (2008) 523–531.
[8] T. Ma, H. Yang, L. Lu, J. Peng, Pumped storage-based standalone photovoltaic power generation system: Modeling and techno-economic optimization, Appl. Energy 137 (2015) 649–659.
[9] A.S. Kocaman, V. Modi, Value of pumped hydro storage in a hybrid energy generation and allocation system, Appl. Energy 205 (2017) 1202–1215.
[10] A.S. Kocaman, Optimization of hybrid energy systems with pumped hydro storage: A case study for Turkey, J. Fac. Eng. Archit. Gazi Univ. 34 (1) (2019) 53–68.
[11] M. Guezgouz, J. Jurasz, B. Bekkouche, T. Ma, M.S. Javed, A. Kies, Optimal hybrid pumped hydro-battery storage scheme for off-grid renewable energy systems, Energy Convers. Manage. 199 (2019) 112046.
[12] B.A. Bhayo, H.H. Al-Kayiem, S.I. Gilani, F.B. Ismail, Power management optimization of hybrid solar photovoltaic-battery integrated with pumped-hydro-storage system for standalone electricity generation, Energy Convers. Manage. 215 (2020) 112942.
[13] N. Lu, J.H. Chow, A.A. Desrochers, Pumped-storage hydro-turbine bidding strategies in a competitive electricity market, IEEE Trans. Power Syst. 19 (2) (2004) 834–841.
[14] A. Borghetti, C. D'Ambrosio, A. Lodi, S. Martello, An MILP approach for short-term hydro scheduling and unit commitment with head-dependent reservoir, IEEE Trans. Power Syst. 23 (3) (2008) 1115–1124.
[15] J. Garcia-Gonzalez, R.M.R. de la Muela, L.M. Santos, A.M. Gonzalez, Stochastic joint optimization of wind generation and pumped-storage units in an electricity market, IEEE Trans. Power Syst. 23 (2) (2008) 460–468.
[16] A.J. Duque, E.D. Castronuovo, I. Sánchez, J. Usaola, Optimal operation of a pumped-storage hydro plant that compensates the imbalances of a wind power producer, Electr. Power Syst. Res. 81 (9) (2011) 1767–1777.
[17] N. Löhndorf, D. Wozabal, S. Minner, Optimizing trading decisions for hydro storage systems using approximate dual dynamic programming, Oper. Res. 61 (4) (2013) 810–823.
[18] O. Bozorg Haddad, P.-S. Ashofteh, S. Rasoulzadeh-Gharibdousti, M.A. Mariño, Optimization model for design-operation of pumped-storage and hydropower systems, J. Energy Eng. 140 (2) (2014) 04013016.
[19] G. Vojvodic, A.I. Jarrah, D.P. Morton, Forward thresholds for operation of pumped-storage stations in the real-time energy market, European J. Oper. Res. 254 (1) (2016) 253–268.
[20] M. Ak, E. Kentel, S. Savasaneril, Quantifying the revenue gain of operating a cascade hydropower plant system as a pumped-storage hydropower system, Renew. Energy 139 (2019) 739–752.
[21] J.-F. Toubeau, Z. De Grève, P. Goderniaux, F. Vallée, K. Bruninx, Chance-constrained scheduling of underground pumped hydro energy storage in presence of model uncertainties, IEEE Trans. Sustain. Energy (2019).

[22] G. Longoria, A. Davy, L. Shi, Subsidy-free renewable energy trading: A meta agent approach, IEEE Trans. Sustain. Energy 11 (3) (2020) 1707–1716.
[23] H. Avci, E. Cigdem Karakoyun, A. Kocaman, E. Nadar, P. Toufani, Integration of pumped hydro energy storage and wind energy generation: Structural analysis and algorithms, Preprint http://dx.doi.org/10.13140/RG.2.2.17949.95200/1.
[24] W.B. Powell, A. George, H. Simao, W. Scott, A. Lamont, J. Stewart, SMART: A stochastic multiscale model for the analysis of energy resources, technology, and policy, INFORMS J. Comput. 24 (4) (2012) 665–682.
[25] Y. Zhou, A. Scheller-Wolf, N. Secomandi, S. Smith, Managing wind-based electricity generation in the presence of storage and transmission capacity, Prod. Oper. Manage. 28 (4) (2019) 970–989.
[26] J.D. Hunt, M.A.V. Freitas, A.O.P. Junior, Enhanced-pumped-storage: Combining pumped-storage in a yearly storage cycle with dams in cascade in Brazil, Energy 78 (2014) 513–523.
[27] J.D. Hunt, M.A.V. de Freitas, A.O.P. Junior, A review of seasonal pumped-storage combined with dams in cascade in Brazil, Renew. Sustain. Energy Rev. 70 (2017) 385–398.
[28] A.F. Ribeiro, M.C.M. Guedes, G.V. Smirnov, S. Vilela, On the optimal control of a cascade of hydro-electric power stations, Electr. Power Syst. Res. 88 (2012) 121–129.
[29] Y. Zhou, A. Scheller-Wolf, N. Secomandi, S. Smith, Electricity trading and negative prices: Storage vs. disposal, Manage. Sci. 62 (3) (2016) 880–898.
[30] B. Steffen, C. Weber, Optimal operation of pumped-hydro storage plants with continuous time-varying power prices, European J. Oper. Res. 252 (1) (2016) 308–321.
[31] B. Zhou, S. Liu, S. Lu, X. Cao, W. Zhao, Cost–benefit analysis of pumped hydro storage using improved probabilistic production simulation method, J. Eng. 2017 (13) (2017) 2146–2151.
[32] H.M. Al-Masri, A. Al-Quraan, A. AbuElrub, M. Ehsani, Optimal coordination of wind power and pumped hydro energy storage, Energies 12 (22) (2019) 4387.
[33] K. Bruninx, Y. Dvorkin, E. Delarue, H. Pandžić, W. D'haeseleer, D.S. Kirschen, Coupling pumped hydro energy storage with unit commitment, IEEE Trans. Sustain. Energy 7 (2) (2015) 786–796.
[34] Y. Ma, C. Li, J. Zhou, Y. Zhang, Comprehensive stochastic optimal scheduling in residential micro energy grid considering pumped-storage unit and demand response, J. Energy Storage 32 (2020) 101968.
[35] K. Kusakana, Optimal scheduling for distributed hybrid system with pumped hydro storage, Energy Convers. Manage. 111 (2016) 253–260.
[36] J. Jurasz, J. Mikulik, M. Krzywda, B. Ciapała, M. Janowski, Integrating a wind- and solar-powered hybrid to the power system by coupling it with a hydroelectric power station with pumping installation, Energy 144 (2018) 549–563.
[37] USGS, USGS water data for the nation help, 2018, https://help.waterdata.usgs.gov/. (Accessed 8 July 2020).
[38] W. Wang, P.H.J.M. Van Gelder, J.K. Vrijling, J. Ma, Forecasting daily streamflow using hybrid ANN models, J. Hydrol. 324 (1–4) (2006) 383–399.
[39] W. Wang, P.v. Gelder, J.K. Vrijling, Periodic autoregressive model applied to daily streamflow, in: Hydroinformatics: (in 2 Volumes, with CD-ROM), World Scientific, 2004, pp. 1334–1341.
[40] G. Tauchen, Finite state Markov-chain approximations to univariate and vector autoregressions, Econom. Lett. 20 (2) (1986) 177–181.
[41] NYISO, Energy market & operational data, 2019, https://www.nyiso.com/energy-market-operational-data. (Accessed 8 July 2020).
[42] J. Hull, A. White, Numerical procedures for implementing term structure models I: Single-factor models, J. Deriv. 2 (1) (1994) 7–16.
[43] P. Jaillet, E.I. Ronn, S. Tompaidis, Valuation of commodity-based swing options, Manage. Sci. 50 (7) (2004) 909–921.
[44] O. Edenhofer, R. Pichs-Madruga, Y. Sokona, K. Seyboth, S. Kadner, T. Zwickel, P. Eickemeier, G. Hansen, S. Schlömer, C. von Stechow, et al., Renewable Energy Sources and Climate Change Mitigation: Special Report of the Intergovernmental Panel on Climate Change, Cambridge University Press, 2011.
[45] Nord Pool, Europe's leading power market, 2021, https://www.nordpoolgroup.com/historical-market-data/.